SANDIA REPORT

SAND2016-9127
Unlimited Release
Printed September 2016

V&V of Residual Stress for GTS

Lauren L. Beghini, Stacy M. Nelson, Kevin L. Manktelow

Prepared by
Sandia National Laboratories
Albuquerque, New Mexico 87185 and Livermore, California 94550

Sandia National Laboratories is a multi-program laboratory managed and operated by Sandia Corporation, a wholly owned subsidiary of Lockheed Martin Corporation, for the U.S. Department of Energy's National Nuclear Security Administration under contract DE-AC04-94AL85000.

Sandia National Laboratories

Issued by Sandia National Laboratories, operated for the United States Department of Energy by Sandia Corporation.

Available to DOE and DOE contractors from
U.S. Department of Energy
Office of Scientific and Technical Information
P.O. Box 62
Oak Ridge, TN 37831

Telephone: (865) 576-8401
Facsimile: (865) 576-5728
E-Mail: reports@adonis.osti.gov
Online ordering: http://www.osti.gov/bridge

Available to the public from
U.S. Department of Commerce
National Technical Information Service
5285 Port Royal Rd
Springfield, VA 22161

Telephone: (800) 553-6847
Facsimile: (703) 605-6900
E-Mail: orders@ntis.fedworld.gov
Online ordering: http://www.ntis.gov/help/ordermethods.asp?loc=7-4-0#online

SAND2016-9127
Unlimited Release
Printed September 2016

V&V of Residual Stress for GTS

Lauren L. Beghini
Stacy M. Nelson
Kevin L. Manktelow
Multi-physics Modeling and Simulation
Sandia National Laboratories
P.O. Box 969
Livermore, CA 94550-0969
llbeghi@sandia.gov

Abstract

Residual stresses induced during forging and welding can cause detrimental failure in reservoirs due to enhanced possibility of crack propagation. Therefore, reservoirs must be designed with yield strengths in a tight range. This report summarizes an effort to verify and validate a computational tool that was developed to aid in prediction of the evolution of residual stresses throughout the manufacturing process. The application requirements are identified and summarized in the context of the Predictive Capability Maturity Model (PCMM). The phenomena of interest that the model attempts to capture are discussed and prioritized using the Phenomena Identification and Ranking Table (PIRT) to identify any gaps in our approach. The fidelity of the modeling approach is outlined and details on the implementation and boundary conditions are provided. The code verification requirements are discussed and solution verification is performed, including a mesh convergence study on the series of modeling steps (forging, machining and welding). Validation activities are summarized, including validation of the displacements, residual stresses, recrystallization, yield strength and thermal history. A sensitivity analysis and uncertainty quantification are also performed to understand how variations in the manufacturing process affect the residual stresses.

Acknowledgment

The advancements in the modeling and simulation capabilities described in this report were only possible because of previous work by others and continued support from ASC P&EM, V&V, and IC programs. ASC P&EM and ASC V&V project management and funding support were provided by Jim Redmond, Jeff Payne, and Arthur Brown.

Previous developments in process modeling for forging, machining, and welding come from many individual and team contributions of the past several years. Arthur Brown, Tim Kostka, Bonnie Antoun, Mike Maguire, Lisa Deibler, Mike Veilleux, Jay Foulk, and Tom Reynolds are a few of the many individuals that have contributed towards the success of this milestone.

Many of the material model developments including dynamic strain aging and recrystallization are a result of research done by Arthur Brown and others. Other facets of the microstructure evolution model have a rich history of development, with credit given to D. Bamman, M. Chiesa, G. Johnson, D. Regueiro, M. Marin, and several others.

The remeshing and state variable mapping (including machining) aspects of this milestone could not have been successful without the programs, processes, and mathematical formalisms tested and developed by Jay Foulk, Mike Veilleux, John Emery, Alejandro Mota, Sofie Leon, and Jake Ostien. Their tools served a foundational role in milestone developments that enabled state variable mapping in complex multi-physics contact problems. Support from Mike Veilleux and Jay Foulk on the use and implementation of these tools was particularly valuable in this regard.

We would also like to acknowledge the support and direction provided by the L2 Milestone review committee including Scott Peterson (chair), Kendall Pierson (code expert), Bill Scherzinger (constitutive model expert), Patty Hough and Sophia Lefantzi (V&V experts), Dorian Balch (GTS customer), and Arthur Brown (multi-physics modeling and simulation (Org. 8259) manager).

Although this project was defined as a joint P&EM and V&V effort there were significant contributions from the integrated code (IC) program. The SIERRA development teams – particularly Solid Mechanics and Thermal/Fluid – provided major support through bug fixes, feature implementation, office hours, and general troubleshooting. Their work on improving solution robustness and implicit contact, in particular, resulted in major improvements during the course of this work that enabled the solution of challenging multi-physics problems that were previously difficult or impossible to solve. This partnership was critical to successful completion of the milestone objectives, and should serve as a model for future milestones.

Finally, the programs supporting this milestone are implicitly part of a larger Predictive Capability Framework Pegpost research effort led by Jay Foulk to simulate the GTS cradle-to-grave life cycle. The Pegpost effort has been valuable in coordinating research efforts that support immediate milestone objectives, discussing and addressing technical challenges, as well as in scoping work to support long-term visions for modeling and simulation capability development.

Contents

List of Figures

List of Tables

Chapter 1

Introduction

Verification and Validation (V&V) is useful for establishing credibility of modeling predictions and assessing potential sources of uncertainty associated with such models. As defined in [11], verification is the process of assessing software correctness and numerical accuracy of the solution to a given mathematical model while validation is the process of assessing the physical accuracy of the mathematical model using comparisons between experimental data and computational results. The purpose of this report is to document both the verification and validation efforts associated with a computational tool developed to model a series of manufacturing processes, including forging, machining and resistance welding. To understand the numerical accuracy of the solution, a mesh convergence study was conducted and determined which level of refinement was necessary for convergence of the residual stress field on each of the three solution steps. From there, the converged mesh was used to conduct a preliminary sensitivity analysis and parameters were selected and tuned based on the customer's input. The critical parameters were then used to quantify uncertainties on the process.

The application for this V&V study is the work flow shown in the first three steps of Figure 1.1: forging, machining and welding, which provides a basis upon which future efforts can be built when a real application needs to be studied for qualification purposes. The work flow and new capabilities studied utilize a series of python scripts and Exomerge [6], C++ programs, CUBIT, and Sierra Aria and Solid Mechanics. The Sierra suite of finite element codes were used for the the finite-element analysis of each process step (forging, machining, or welding). Individual steps are linked through a series of custom python (and BASH) scripts that manage job submission and termination, transfer material state and residual stress from one step to the next, and post process results.

Individual elements in the GTS lifecycle depicted in Figure 1.1, such as forging or machining, have been modeled and validated [13]. For example, the forging process utilizes a simplified "wedge" that has been validated in previous efforts (described in more detail in Chapter 6). The work described in this report and a companion report [7] builds on these previous efforts by developing, verifying, and validating tools that extend simulation capabilities to resistance welding and subsequent cooling processes. Various proof-of-capability geometries were developed to exercise state transfer tools and evaluate mesh convergence during remeshing and mapping simulation steps. A prototype (simplified) resistance forge weld geometry was selected with the GTS customer that is intended to represent the relevant physics, processes, and geometry used in GTS reservoir manufacturing. Chapter 4 provides additional detail on the machining and analysis of the

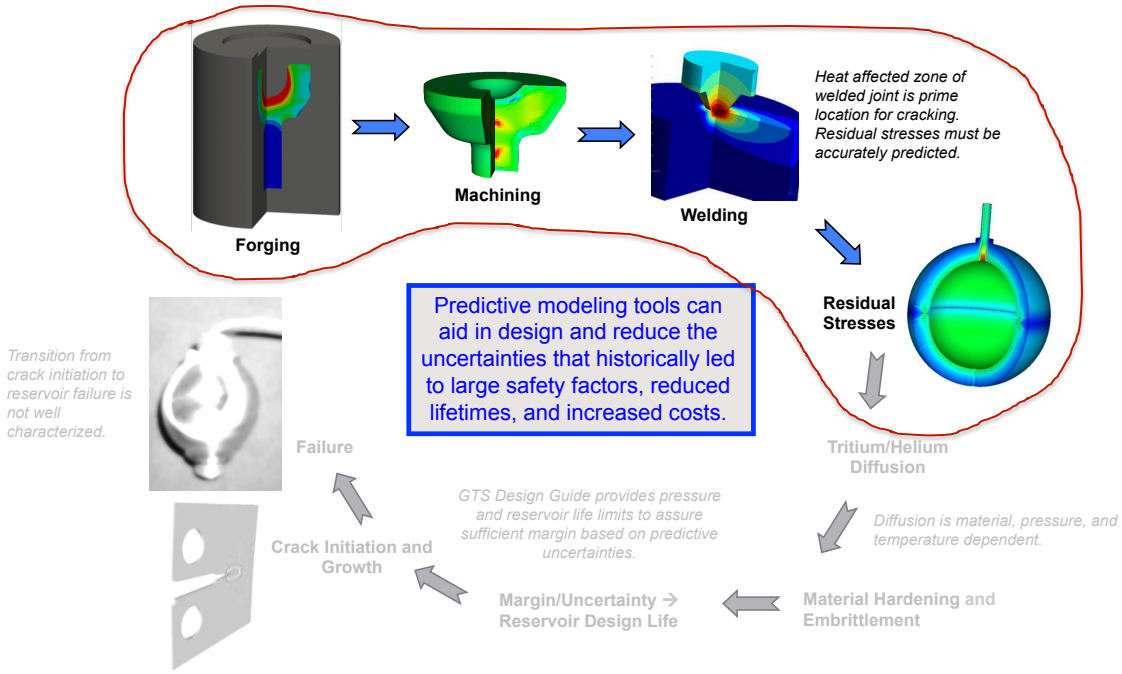

Figure 1.1. GTS Lifecycle Modeling and Simulation (Image courtesy of Arthur Brown)

prototype resistance forge weld geometry.

The primary motivation for this study is to derive a better understanding of how residual stresses induced from previous simulation steps influence a final configuration. High pressure reservoirs manufactured for gas transfer systems (GTS) are an ideal motivating application of such a process sequence, since material properties and residual stress states may change dramatically from step to step. Although GTS reservoir manufacture is generally a well-understood understood process, variability introduced through manufacturing steps and the net residual stress state on a final product can have consequence for qualification testing or result in non-conformances during production. A predictive capability for the entire GTS lfiecycle would be helpful to assess variability, help in SFI investigations, and enable future GTS reservoir designs without long-term shelf storage programs.

Chapter 2

Application Requirements

2.1 Identify requirements

The predictive capability developed here and in [7] is intended for use by Gas Transfer Systems (GTS) on a wide range of problems, where the motivation for the modeling effort is to aid in design and reduce the uncertainties that lead to large safety factors, reduced lifetimes and increased costs. Therefore, the verification and validation aspect of this work is primarily focused on assessing the credibility of the basic model developed to understand the forging, machining and welding steps of the manufacturing process that occur at the initiation of the lifecycle of GTS reservoirs. This work will provide a foundation on which future efforts can be built as work comes into play. As such, a general infrastructure to meet requirements is provided and a path forwards is suggested for adding future work, such as specific applications or incorporation of subsequent steps of the lifecycle (refer to Figure 1.1).

2.2 Model Credibility (PCMM)

The predictive capability maturity model (PCMM) assessment is used to assess the credibility of the modeling predictions [10, 11]. The assessment is broken down by categories in the following text and tables.

Code verification (CVER)

As the code verification element is used to assess the quality control of the software, the desired levels of adequacy were all rated as 2, including the technical review, as the panel of L2 Milestone experts are reviewing this work. For the manufacturing process modeling studied here, apart from a few python scripts and post-processing tools, the analyses were conducted using Sierra Aria and Sierra Solid Mechanics (both implicit quasistatic and explicit dynamics capabilities). Thus, in terms of the levels of code verification achieved, the memo written by the Sierra product owners in [12] provides evidence for the scores listed in Table 2.1 CVER1 to CVER4. Technical review of the code verification activities (CVER5) receives a score of 2 due to the committee reviewing this

work.

Table 2.1. Code verification PCMM element

Code Verification (CVER)		Desired	Achieved
CVER1	Apply Software Quality Engineering (SQE) processes	2	2
CVER2	Provide test coverage information	2	2
CVER3	Identification of code or algorithm attributes, deficiencies and errors	2	0
CVER4	Verify compliance to Software Quality Engineering (SQE) processes	2	2
CVER5	Technical review of code verification activities	2	2

Physics and Material Model Fidelity (PMMF)

The physics fidelity is described in Table 2.2. The desired and achieved level of maturity for characterizing completeness versus the PIRT was selected at 2, which represents that most relevant models in the capability are correlated with the PIRT for the intended application. The behavior listed in the PIRT (see Table 3.2) was also observed. In terms of quantification of the model accuracy, a level of 2 was desired and achieved, which represents some quantitative validation characteristics and conclusions. These validation activities, discussed in Chapter 6 proved the model correctly predicted displacements and general trends in the residual stresses, providing some level of confidence that the fidelity of the physics is reasonable for the application. Sub-element PMMF3 was not addressed as since the capability developed here was for a generic future application, there is no formal validation domain. The physics and/or material model was reviewed by a technical committee, thus justifying a score of 2.

Table 2.2. Physics and Material Model Fidelity PCMM element

Physics and Material Model Fidelity (PMMF)		Desired	Achieved
PMMF1	Characterize completeness versus the PIRT	2	2
PMMF2	Quantify model accuracy (i.e., separate effects model validation)	2	2
PMMF3	Assess interpolation vs. extrapolation of physics and material model	N/A	N/A
PMMF4	Technical review of physics and material models	2	2

Representation and Geometric Fidelity (RGF)

For the process modeling analyzed in this report, we elected to use a simplified geometry that would be representative of a GTS geometry. Though the simplifications make the geometry quite different, the problems we chose have most of the features of a real model. Therefore, the level of maturity desired and achieved for the geometric fidelity is 1. The geometry would need to be updated for the predictions made here to be numerically significant, rather than capturing the general trends. The sensitivity of the solution to major features was not studied as the geometry is a surrogate for future applications. The problem presented here was chosen to demonstrate capability, thus studying the sensitivity was outside of the scope. The geometry was reviewed but not certified by the customer, giving sub-element RGF3 justification for a score of 2.

Table 2.3. Representation and Geometric Fidelity PCMM element

Representation and Geometric Fidelity (RGF)		Desired	Achieved
RGF1	Characterize representation and geometric fidelity	1	1
RGF2	Geometry sensitivity	N/A	N/A
RGF3	Technical review of representation and geometric fidelity	2	2

Solution verification (SVER)

The solution verification, one of the primary areas of focus of this work, is used to assess and explain the error in our numerical solution. SVER1 receives a score of 2 (both achieved and desired) since a formal convergence study was conducted to assess the effects of mesh discretization on the predicted residual stress, the main quantity of interest. We observed small changes and trend consistencies in the residual stress across multiple fidelities. More details of the mesh convergence study are given in Section 5.2.1. The uncertainty in the numerical error was not studied as it was outside the scope of this work; thus, the corresponding desired and achieved levels are both reported as 0. For SVER3, verification of the simulation input decks, the desired level of 2 was achieved by inspection of one or more people other than the analyst(s), which included code developers. While an ideal score of 2 corresponds to independent review of the post-processor input decks for the intended application for SVER4, they were in actuality inspected only by the team of analysts, thus receiving a score of 1. Technical review was conducted by the independent L2 Milestone committee, thus justifying a score of 2.

Table 2.4. Solution Verification PCMM element

Solution Verification (SVER)		Desired	Achieved
SVER1	Quantify numerical solution errors	2	2
SVER2	Quantify uncertainty in computational (or numerical) error	0	0
SVER3	Verify simulation input decks	2	2
SVER4	Verify simulation post-processor input decks	2	1
SVER5	Technical review of solution verification	2	2

Validation (VAL)

The validation hierarchy was not formally defined as a specific application has not been identified. Consequently, the validation table was omitted from the scope of this work, but the validation activities associated with our workflow are discussed in Chapter 6.

Uncertainty quantification (UQ)

The uncertainty quantification (UQ) is performed to assess the various sources of uncertainty present in the model. The uncertainties were identified and characterized in Chapter 7, giving justification for a UQ1 score of 1 since separation (segregation, etc) was not performed. For UQ2, a qualitative sensitivity analysis was performed justifying a score of 1 for UQ2, though the desired score is 2, which can be achieved by performing a quantitative sensitivity analysis of some of the uncertainties. The impact of aleatory/epistemic uncertainties was performed, but without separation, justifying a score of 1 in both the desired and achieved categories of UQ 3. Aggregation or roll-up of the numerical and physical model parameter uncertainty at one level was desired and performed, resulting in a maturity level of 2 for UQ4. UQ5 again reports a maturity level of 2 since technical review was conducted by the independent L2 Milestone committee.

Table 2.5. Uncertainty Quantification PCMM element

Uncertainty Quantification (UQ)		Desired	Achieved
UQ1	Aleatory and epistemic uncertainties identified and characterized	1	1
UQ2	Perform sensitivity analysis	2	1
UQ3	Quantify impact of uncertainties from UQ1 on quantities of interest	1	1
UQ4	UQ aggregation and roll-up	2	2
UQ5	Technical review of uncertainty quantification	2	2

Chapter 3

Phenomena Identification and Ranking Table

The Phenomena Identification and Ranking Table (PIRT) is used to identify and prioritize physical phenomena in an application and assess associated gaps or inadequacies in the modeling approach to ensure sufficiency and efficiency [16]. In this chapter, we discuss the most significant phenomena for each of the forging, machining and welding processes and how well the model is able to capture the behavior using the PIRT.

3.1 Phenomena

Forging

The forging process (described in more detail in Chapter 4) was developed to understand the evolution of residual stresses throughout the manufacturing process. Thus, the most important criteria include tracking the microstructure evolution due to the high temperature manufacturing process and demonstrating the buildup of residual stress. In order to accurately capture the microstructure evolution, the material model used in this work is a high-rate and high-temperature plasticity model, described in [1]. This material model allowed for multiple cycles of static and dynamic recrystallization and was necessary to predict yield strength. Since forging occurs at high temperatures, the material model also needed to account for thermal expansion and heat due to plastic dissipation and ensure proper radiation, convection and conduction boundary conditions were applied to have accurate residual stresses. These phenomena are of particular importance as they are also included in the L2 Milestone completion criteria for FY16 [7].

Machining

Likewise, in modeling the machining process, the behavior of highest importance that we aim to capture is the deformation due to relaxation of the residual stress field, similar to what was observed experimentally using the contour method. For the modeling, however, the methodology in which a part is ”machined” consists of creating a mesh of the machined geometry and then mapping the

state from the unmachined geometry over and allowing the new mesh and imposed state to come to equilibrium. In order to observe realistic behavior, it is necessary to have a robust process to map and transfer the state, which was developed in [8] and now implemented in Sierra SM production code. Previous efforts, discussed in more detail in Chapter 6, utilized MAPVAR [17], which was less robust and based on averaging the fields at a specific location. The conversion over to the new methodology occurred in FY16.

Welding

The simplified resistance forge weld was modeled to demonstrate a representative GTS problem where a stem and reservoir would be machined out of a cup and stem forging. The oversized stem would then be inserted into a base while current is applied and softening occurs. Therefore, the phenomena we aim to capture with this simplified problem would need to demonstrate the behavior present in a real model. Most importantly, implicit contact is needed to capture the interaction between the stem and base to capture the deformation field while ensuring that no interpenetration occurs, though when implicit contact fails, explicit contact might be explored as a workaround. As current is applied, it is important to capture Joule heating as temperatures approach near melt conditions. The material must respond accordingly and soften or harden as temperatures increase or decrease respectively. Finally, experiments have shown that a proper weld has grain growth across the interface between the stem and base, thus our model must capture bonding across the contact interface to be consistent.

3.2 Requirements

In Table 3.2, the green shows that there are no gaps between the model and the intended importance level, yellow shows one level of difference between the model and its importance level and red illustrates two levels of difference. The majority of the phenomena were well represented, achieving the same level as intended (green), but some inadequacy was noted for the validation category, especially for the resistance welding. Plans are underway to address these issues in FY17.

3.3 Adequacy

Mathematical Model Adequacy

A high mathematical model adequacy indicates that a mature physics-based model is available which represents the phenomena over the full parameter space of the application, while a level of medium corresponds to at least one model form that nominally captures the phenomenon over

Table 3.1. Phenomena Identification and Ranking Table (PIRT) for Forging, Machining and Welding Process

Phenomena	*Imp*	Math Model	Code	Validation
Forging	H			
Microstructure evolution due to high temperature manufacturing process	H	H	H	M
Buildup of residual stress	H	H	H	M
Conduction, radiation, convection and heat due to plastic dissipation and associated thermal expansion	H	H	H	M
Multiple cycles of static and dynamic recrystallization	H	H	H	M
Prediction of yield strength	H	H	H	M
Machining	H			
Remap and transfer of material state	H	H	H	L
Relaxation of residual stress	M	M	M	M
Welding	H			
Implicit contact	M	M	M	L
Bonding across the interface	H	M	M	L
Material hardening/softening with temperature	H	H	H	L
Joule heating	H	H	H	M

some portion of the application parameter space [16]. The majority of the phenomena we aimed to capture had mathematically adequate models in place, thus achieving their desired rank of high and highlighted in green. One inadequacy in the mathematical model was the implicit contact. Implicit contact algorithms and associated mathematical models attempt to simultaneously enforce interpenetrability constraints, force balance, and complex friction models on an unknown future geometrical configuration. This is a challenging problem for any finite-element code. The mathematical model adequency is rated to reflect this deficiency and highlight the need for future work. Mathematical models for frictional interface enforcement are rudimentary, and contact enforcement algorithms permit non-phsyical stress oscillations along interfaces.

Code Adequacy

The majority of the phenomena in Table 3.2 list a high level of adequacy in terms of the code, which indicates the intended model is implemented in Sierra. Furthermore, Sierra has a test suite in which similar problems are run routinely (nightly), and verification problems have been run that test the correctness of the numerical implementation. There are no outstanding (reported) bugs or issues that can undermine usage of the model, though we note that as this process was developed, several bugs were reported and resolved to improve the robustness.

The categories in which a difference of one level of required importance verses adequacy is reported (in yellow) include implicit contact during the welding process, and relaxation of residual stress in the machining step. This is because the models are implemented in the code, but the capabilities are not fully functional.

A significant amount of effort was devoted to evaluating the implicit contact algorithm and noting areas for potential improvement during the course of this work. Several bugs and areas for improvement were identified and reported to the SIERRA Solid Mechanics development team. During FY16, a close partnership with the development team fostered a number of significant improvements in contact convergence and accuracy were made that enable solution of previously impossible or challenging problems. Resistance welding simulations, for example, previously failed to converge but are now capable of running to near completion. There is still significant room for improvement in what is recognized as a difficult problem. Frequently, as boundary conditions are modified or the mesh geometry slightly perturbed, the contact algorithm fails to converge. Thus, Table 3.2 reports that the adequacy is still below the requirement and reflects the need for future partnerships between analysts and code developers to study implicit contact.

Residual stress for the machining process is rated to reflect convergence issues and unreasonably long run times. The process is best described using a quasi-static mathematical model and solution process. However, convergence and run time issues necessitate the use of explicit dynamics code with significant mass scaling as a work-around solution. Mass scaling (and other techniques to increase the critical time step) is an undesirable solution because it requires providing non-physical parameters to an otherwise highly adequate mathematical model. The authors acknowledge that robustness has improved, and have started exploring the use of a newly-developed capability called explicit-quasistatic mode for some steps in the process. Explicit quasi-static mode

uses a combination of mass-scaling and viscious dissipation strategies to arrive at a nominally quasi-static solution. Future work and investigation in using explicit quasi-static mode will continue into the next FY as an alternative to implicit solutions where convergence challenges remain.

Validation Adequacy

Validation activities for this work have been somewhat limited, therefore, most levels are lower than desired. A level of medium denotes partial validation support but a lack of statistical comparison of experimental data, whereas a level of low represents insufficient validation support for the model use, which could include a comparison of experiment "pictures" with prediction [16]. Previous work described in [3, 13, 2] discusses the validation of the forging simulation for a wedge, cup and stem and U-cup, where the microstructure evolution was validated over a range of temperatures and applications. The machining validation activities included validation of the displacement of a wedge in which tensile specimens were machining away and the relaxation was measured. This activity is discussed in more detail in Section 6.2. In terms of the welding process, no experiments have been conducted and compared with the model to date. However, the Joule heating capability was validated for a tapered bar in [5], providing evidence for a level of medium. Plans are currently underway to perform more validation activities in FY17 targeted specifically at the resistance forge weld and machining processes to help improve the gaps identified here.

Chapter 4

Application Model Development

4.1 Geometry definition and fidelity

The application chosen for evaluating the GTS Lifecycle is forging, machining and subsequent resistance forge weld. The resistance forge weld is a solid state weld produced through resistance heating and subsequent cross-boundary recrystallization. This process is relevant for joining a stem to a high pressure bottle. A representative geometry is illustrated in Fig. 4.1, but refer to [7] for additional details. The majority of the deformation in this process occurs at the interface between the stem and bottle. A copper electrode simultaneously passes current flux through the stem and supplies pressure, forcing the stem and bottle together. Therefore, to focus effort on the relevant physics the geometry was simplified. The bottle geometry was approximated using a small portion near where the stem is inserted. The stem was simplified by truncating a portion of the stem tube far away from the major deformation. The electrode geometry is nominally identical to a copper ring electrode used in previous tests. These adjustments were made to reduce computation time with the assumption that additional geometry results in negligible far field effects. Aside from these approximations, the stem and bottle geometry is identical to nominal dimensions on CAD drawings for parts that have been physically tested.

Axisymmetry was further employed to reduce the size of the model. SIERRA does not support axisymmetric elements, so instead a one degree "wedge" was sliced from the full geometry (and supplied with appropriate boundary conditions). This provided a significant advantage in that a surface mesh could be swept through the entire geometry with minimal geometry decomposition.

4.2 Meshing and re-meshing approach

A parameterized CUBIT journal file was used to construct and mesh both the forging and resistance forge weld geometries. The location of large deformation gradients, current fluxes, and temperature distributions is known a priori to exist near the resistance weld region on the interface between the bottle and stem. The mesh size was decreased in this region to help resolve these gradients. As the solution progresses, large deformations lead to element quality deterioration that triggers the remeshing and mapping process.

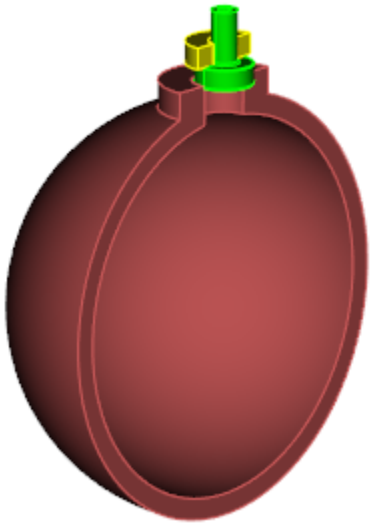

Figure 4.1. Representative/surrogate geometry for a resistance forge weld application.

Remeshing was also accomplished through a custom Python script. The remeshing Python script differs from the original CUBIT meshing and geometry journal file primarily in that mesh-based geometry must be used. Exodus entities (Blocks, Sidesets, and Nodesets) were strategically created in the original journal file so that subsequent remeshing can be precise. For example, a sideset with ID 25 will always create a mesh-based geometry surface with ID 25. Therefore, an appropriate mesh size can be assigned to specific locations in the model.

The lack of actual geometric entities and desire for an automatic and robust remesh process presents a number of challenges. One of these challenges is an unknown deformed geometry must be remeshed, but without opportunity for the traditional geometry decomposition or simplification process. For example, very small features or sharp angles result in areas prone to poor element quality. Such issues can often be resolved by decreasing the mesh size. Therefore, the automated remeshing script contains provisions to evaluate the mesh quality in each area and adjust as appropriate. If poor mesh quality is found, the script will delete the bad mesh, decrease the element size, and attempt several more times until a preset minimum mesh size is reached (at which point the process aborts).

This adaptive all-hexahedral meshing approach is versatile, robust, and well-suited to the specific application problem. Hexahedral remeshing requires additional attention but generally provides reduced element count relative to a tetrahedral mesh. More complex geometries and actual problems, however, may require the use of tetrahedral meshing schemes.

4.3 Material assignment and calibration

The wedge geometry forging and the resistance weld stem and base are machined from 304L stainless steel. The BCJ_MEM constitutive model described in [1] was assigned to each of these parts to model mechanical properties. The parameters for the BCJ_MEM constitutive model were calibrated to test data from B. Antoun, et al. [3, 2]. A summary of some of the test data is depicted in Fig. 4.2. The calibrated material model matches rate and temperature-dependent tests and also models the static and dynamic recrystallization necessary for resistance weld models. The copper electrode was also assigned the same 304L mechanical properties due to current limitations in the remeshing and state variable mapping approach. This limitation should be alleviated in the future as the SIERRA support for internal state variable mapping increases. The thermal and electrical material models used temperature-dependent thermal and electrical conductivities and specific heat. More details on the functional forms and material properties for the resistance forge weld can be found in [7].

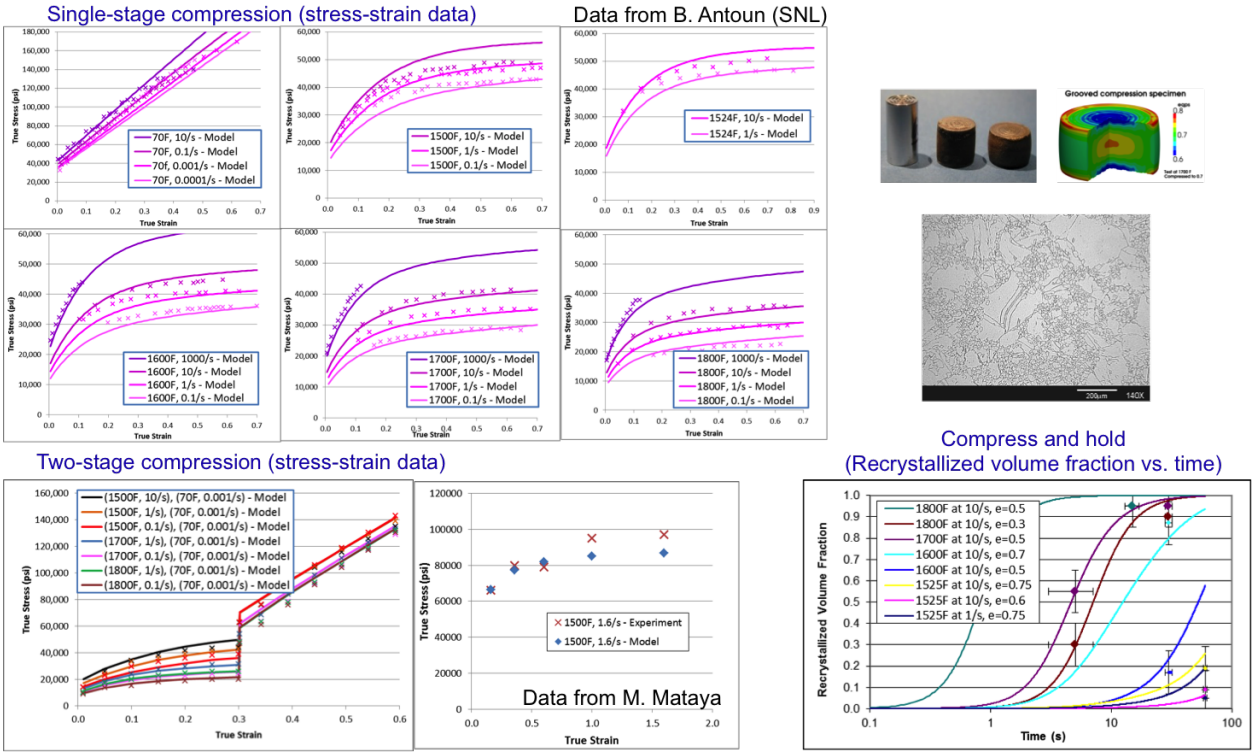

Figure 4.2. Parameter determination for 304L

4.4 Initial conditions and boundary conditions

Modeling the GTS Lifecycle requires a series of simulation steps as depicted in Fig. 1.1. A series of steps was modeled for the forging process, with boundary conditions well-defined based on the testing apparatus. Within the forging process, a number of sub-steps were used to model furnace heating, cooling during transfers to the forging die, an initial forging process, heat treatment, etc. The initial conditions in each process were determined by the final state of the previous step so that residual stresses and internal state variables are transferred and evolve throughout the process.

Resistance forge welding and subsequent residual stress evolution is the final step in the portion of the GTS Lifecycle considered herein. Figure 4.3 diagrams the relevant boundary and interface conditions. The Base is fixed at all degrees of freedom on the bottom edge as an approximation for actual test fixture boundary conditions. In reality, a more sophisticated fixture holds the pressure vessel. In addition, wedge-like periodic boundary conditions are used to model the axisymmetry. The "wedge" boundary conditions are fairly elaborate in that they prevent out-of-plane displacements as well as enforce perfect axisymmetry using multi-point constraints. Each node on the front plane of the assembly is constrained in the axial and radial directions the matching node on the back plane. This provides a reasonable approximation to a 2D axisymmetric element.

The interface of the stem to the base is defined with simple Coulomb friction contact with a coefficient of $\mu = 0.1$. Resistance welding is modeled using a node variable-dependent friction interface that switches to tied after the primary (first) recrystallization cycle reaches a 50% volume fraction. Hence, during the welding process some portions of this interface are tied while others remain free to slip. Thermal and electrical conduction at this interace is assumed ideal. Although previous modeling attempts have used pressure-dependent interface conductivity, this additional level of detail was removed to eliminate sources of model form error at this time.

The electrode is "tied" to the stem. Physically, this is a frictional interface. However, the tied stem increased the solution robustness by reducing the number of frictional interfaces necessary to resolve during implicit contact iterations. Electrical and mechanical loads are supplied through the electrode in the form of applied pressure and current flux (see [7] for additional details). The entire assembly is assumed initially at room temperature (294K).

After the resistance welding process, the entire assembly is allowed to cool with heat leaving through a prescribed temperature boundary condition. This is an additional simulation with initial conditions defined by the final stress state of the resistance forge weld. Residual stresses evolve during this cooling process and can change significantly as materials strain due to thermal expansion and contraction. Future modeling should better capture the thermal conduction, convection, and radiation from exposed boundaries. The basic prescribed temperature boundary condition was sufficient for demonstrating proof-of-concept process modeling.

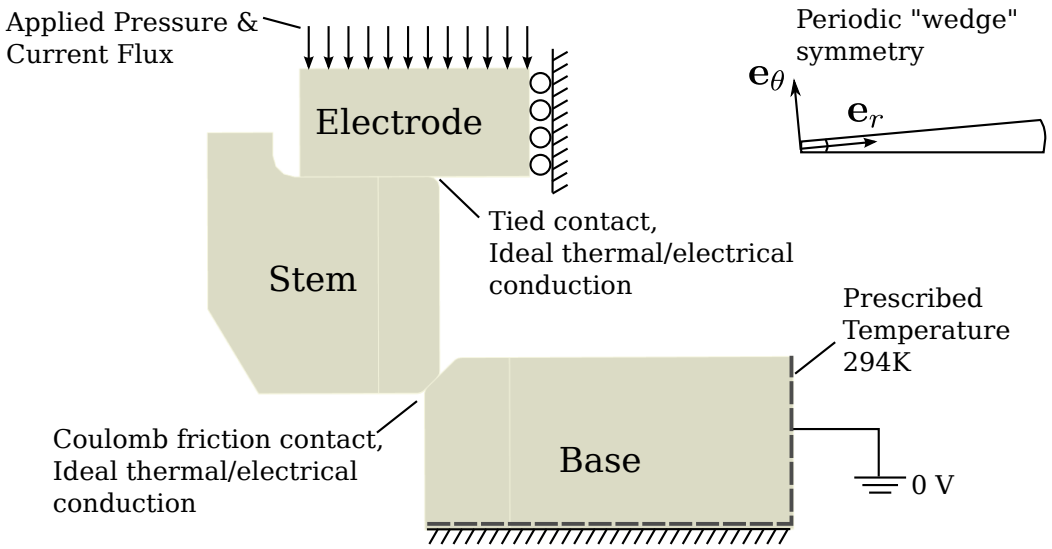

Figure 4.3. Boundary conditions for representative application problem. See [7] for more details.

4.5 Numerical simulation tools

The capability to model the manufacturing processes described here primarily utilizes Dakota, SIERRA/Thermal (Aria) and SIERRA/SM (Solid Mechanics, Adagio). The thermal, electrical, and mechanical physics regions are loosely coupled through the Arpeggio executable. That is, a converged solution from one time step (e.g., Thermal) is passed through to the the next step (e.g., Mechanical). Temperatures or displacements are transferred or interpolated as needed to update material properties, contact or conduction boundaries, etc. A number of other custom Python scripts, as well as the Python-based Exomerge [6] utility were used in driving simulations, remeshing and mapping routines, and automating and monitoring process step sequences.

Chapter 5

Application Verification

5.1 Code Verification Requirements

Code verification activities help build confidence in the solutions obtained from our codes. In this case, *codes* refers to the multitude of finite element codes (Adagio and Aria), coupling tools (Arpeggio), Python scripts (remeshing and mapping drivers, process simulation tools), mapping tools, and material constitutive models. Code verification is inherently a team-based effort in this environment due to the large and diverse SIERRA user base. Hence, there is an entire library of pre-existing verification and validation tests, regression tests, etc. that are foundational to the finite element codes used. Several additional code verification activities helped catch bugs and improve confidence in the correctness of our solutions. These activities fall into three categories: (1) material constitutive model testing, (2) remeshing and mapping tool testing, and (3) code capability testing.

Material constitutive model and remeshing/mapping tool testing were necessary activities due to new or modified codes. *Code capability* testing includes those activities designed to gain confidence in existing (and theoretically tested) foundational code capabilities such as implicit contact. In many cases, code capability testing also improves understanding of the code and its limitations to prevent erroneous or unintended usage.

Material constitutive model tests were necessary due to enhancements to the BCJ_MEM material model. The BCJ_MEM material constitutive model provides microstructure evolution modeling capabilities required to model hardening, recrystallization, grain growth, and recovery mechanisms. The BCJ_MEM model has long been part of the verified, validated, and tested production code in SIERRA (actually, in Lamé). However, the original BCJ_MEM model was also written in FORTRAN and had some fundamental implementation details that hindered further development. In some problems, BCJ_MEM could not solve the complex evolution equations and instead used a simple radial return approximation leading to incorrect solutions. For these reasons, the BCJ_MEM material model was converted to C++ (the language used for a majority of SIERRA) and the resulting development model was named *DSA* since the original intent was to add a dynamic strain aging (DSA) capability. As the BCJ_MEM model was converted from FORTRAN to C++, several of the other implementation details were also improved to help provide robust solutions in situations where the internal BCJ_MEM solver may have previously stalled.

Several verification and regression tests were added to the nightly SIERRA test repository during this process, making the DSA material model more tested than any similar model (e.g., BCJ_MEM or elastoviscoplastic). The DSA material model was developed originally using all of the previous verification and regression tests for the BCJ_MEM material model. "Gold" results files generated from the original BCJ_MEM material model were used as a basis, ensuring that any new code produced an identical solution to within very tight tolerances (often less than 1e-10 relative tolerance). A summary of these additional tests follows:

- 5 abnormal usage tests transferred from BCJ_MEM ensure valid model input and parameter specification
- A localization patch test transferred from BCJ_MEM to test average pressure formulation for locking
- 2 localization tests transferred from BCJ_MEM for a uniaxial tension condition (with and without initial grain size, recrystallization, hardening, and damage parameters)
- 2 damage evolution tests transferred from BCJ_MEM
- Grain size effects regression test transferred from BCJ_MEM
- Recrystallization evolution test transferred from BCJ_MEM, and modified to include multi-cycle recrystallization
- Four element-level shear regression tests testing multiple shear directions in both explicit quasi-static and implicit solution modes with the selective-deviatoric elemement formulation.
- 4 element-level tension regression tests testing multiple constitutive model solvers (original re-coded BCJ_MEM solver as well as a new, more robust DSA solver), implicit solution, explicit solution, and explicit quasi-static solution options
- 4 additional tension and shear tests at multiple strain rates to verify that the DSA material model also replicates the elastoviscoplastic material model.

These verification and regression tests played a critical role in the DSA material model development process, and even helped find (and fix) several bugs in the production BCJ_MEM material model. As a result, the conversion and model develpoment of DSA can also be regarded as a thorough peer-review of the BCJ_MEM model.

Several C++ and Python tools used for mapping material state variables were also developed as part of this effort. These tools were used during remeshing steps or machining simulations. The state variable mapping process is a sequence of steps that requires parsing user input, tensor logarithm and exponentials, interpolation, and mesh modification. Individual steps in this process as well as combined steps were tested in a development repository, separate from the production SIERRA tests. Tests included machining with multiple blocks and multiple element types, reading input files with various attributes, mesh push forward (with and without updating the reference configuration), gauss point interpolations (mappings), and combinations of steps requried for a complete remesh. These tests helped during the development of a remeshing python script and with debugging of a series of custom C++ state variable mapping tools (written by Mike Veilluex, Jay Foulk, John Emery, and others). These python scripts were a required (but intermediate) step in developing a production remeshing and mapping capability. The SIERRA development team

has since implemented a state variable mapping tool internal to SIERRA that is now tested and verified nightly.

Lastly, several quick-running example problems were studied during the development of the remeshing and machining process in order to assess core capabilities. Capabilities assessed include basic functionality in SIERRA such as implicit contact, element types, and code coupling as well as remeshing and mapping scripts and tools.

Figure 5.1 illustrates one example problem used in assessing the remeshing and mapping process errors. An initially undeformed block of material is subject to pressure loads that cause major plastic deformation. The pressure loads are transmitted through a nearly rigid top die, resulting in large plastic deformations in the main block and bottom die. Figure 5.1 depicts the plastic strain evolution at an intermediate time step. This example exercises physics encountered in larger problems such as plain strain boundary conditions, implicit frictional contact, high stiffness contrasts, plasticity, and surface traction loads as well as numerical parameters such as element type, solver parameters, coupled codes, etc. Furthermore, it exercises the remeshing scripts and tools to an extreme level – mapping and remeshing at every converged time step.

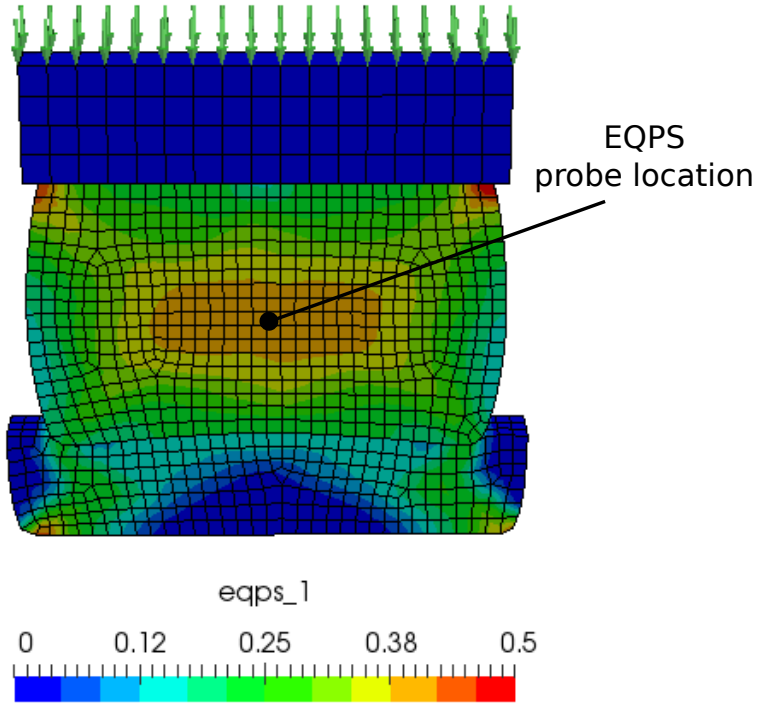

Figure 5.1. "Cube crush" demonstration problem verifying the accuracy of repeated remeshing and mapping process scripts and mapping tools.

A quantitative comparison of the error incurred during a sequence of remeshing and mapping steps is provided in Fig. 5.2. The quantity of interest was plastic strain at the center of the

main block, where the maximum equivalent plastic strain (eqps) is observed. Two solution processes were compared: a reference/baseline solution without remeshing, and a solution which was remeshed and mapped at each converged time step. The expectation is that the two plastic strain curves (as a function of time) are nearly identical, and this is exactly what was observed. Note that the baseline solution stops just prior to t=0.25s. This is because the initial mesh fundamentally limits the amount of deformation that can occur before elements invert and cause solution failure. Small deviations are expected and may be attributed to mesh irregularity due to remeshing, and potential errors in the internal state variable mapping process. Errors due to the latter were explicitly evaluated. After each converged time step, the equivalent plastic strain ε^p (probed at the block center) was compared to the plastic strain after cycling through the remeshing and mapping process. The relative error was computed according to

$$\varepsilon_e^p = \frac{\varepsilon_f^p - \varepsilon_i^p}{\varepsilon_f^p} \times 100\%, \tag{5.1}$$

where ε_f^p is the "final" plastic strain after a remeshing sequence (including an equilibrium step), and ε_i^p is the "initial" plastic strain, just before the remeshing and mapping sequence begins. As seen in the bottom graph of Fig. 5.2, the remeshing and mapping process introduces very little error in the plastic strain variable – less than 1% at each time step. Additional tests like this one would be beneficial in better understanding the overall errors that may be attributable to the remeshing and mapping process. For example, the equivalent plastic strain is a relatively smoothly evolving gauss point field with a limited range (generally greater than 0 and almost always less than 10 for most problems). However, other internal gauss variables and internal state variables may span several orders of magnitude, be discontinuous in places, or may only take on discrete values, for example. These additional cases deserve a more in-depth study. Nevertheless, the remeshing and mapping process has been quite effective on several problems and close examination of mapped results in combination with basic code verification testing indicates the intended solutions are being obtained.

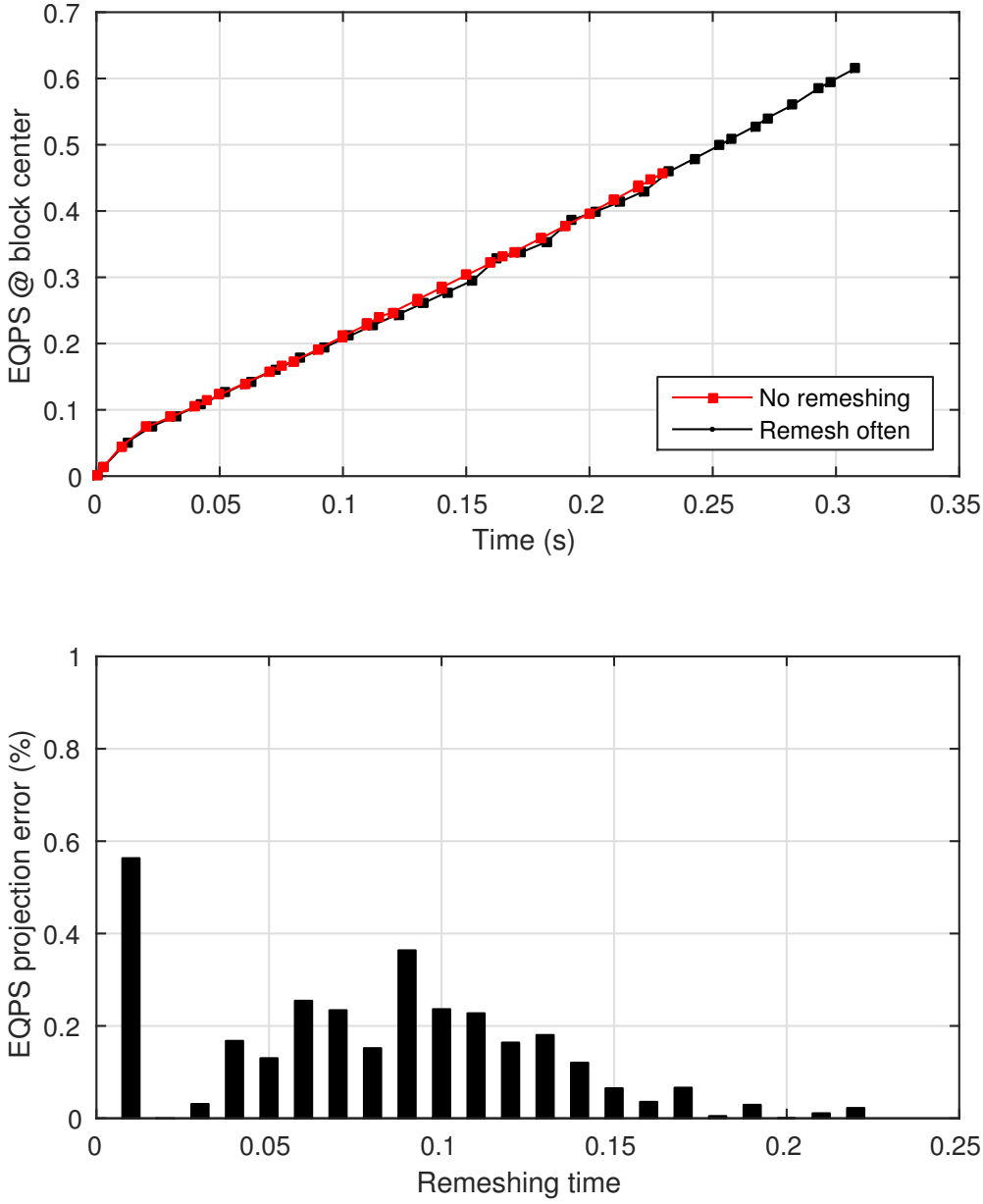

Figure 5.2. (top) Equivalent plastic strain evaluated at the center of the crushed block compared between a baseline solution (no remeshing) and between a solution passed through the remeshing and mapping scripts at every time step. (bottom) Equivalent plastic strain error developed through the mapping process at each step.

5.2 Solution Verification Approach

Solution verification activities were completed to quantify the numerical errors associated with the relevant stresses predicted throughout the simulated forging/machining/welding process. A common source of numerical error arises during the development of a finite element simulation as the differential equations representing the modeled process undergo conversion into an algebraic system of equations representative of the simulated geometry's lattice, or mesh. This discretization process introduces a discretization error closely associated with element size, as a lattice made progressively coarser becomes respectively less characteristic of the continuous variables it is meant to represent. Consequently, in order to make confident prediction with a finite element simulation, the discretization error must be quantified and shown to be of an acceptably low level. Furthermore, extrapolation-based error estimation techniques can be applied during the computer simulation process to estimate a model's continuum solution, or the solution corresponding with an element size of zero, that can be compared with discrete solutions in order to develop the discretization errors. Therefore, an extrapolation-based error estimation technique was applied during the simulated forging/machining/welding process to determine the mesh related discretization errors, as well as the maximum acceptable element size permitting confident stress predictions throughout this simulated manufacturing process.

5.2.1 Quantify Numerical Error

As discussed, in the process of making predictions with computer simulations, the associated numerical errors must be minimized in order to have confidence in the predicted quantities of interest. Therefore, the discretization errors associated with the estimation of the residual stresses throughout each of the proposed forging, machining, and welding processes were determined with a mesh convergence study based upon the Richardsons extrapolated exact solutions.

Richardsons extrapolation, which is an extrapolation-based error estimation technique, allows for the approximation of a higher order estimate of a continuum solution given a series of lower order, discrete solutions [14, 15]. As shown in Eq 5.2, with this technique, a discrete solution, f_k, can be thought of as the exact solution plus some error terms:

$$f_k = f_{exact} + g_1 h_k + g_2 h_k^2 + g_3 h_k^3 + \ldots \tag{5.2}$$

Where g_i represents the i-th term error coefficient and h_k represents a measure of the grid spacing, or element size. Then, if a second order method is assumed ($g_1 = 0$) for the above equation and if the discrete solutions exist for at least two different mesh sizes, the above equation can be solved for the exact, or continuum, solution with Eq. 5.3:

$$f_{exact} \approx f_1 + \frac{f_1 - f_2}{r^2 - 1} \tag{5.3}$$

Where r is the ratio of grid sizes, h_2/h_1 , and f_k represents the two discrete solutions. Then, the Richardson extrapolation given by the above equation can be generalized for any pth order method (Eq. 5.4):

$$f_{exact} \approx f_1 + \frac{f_1 - f_2}{r^p - 1} \tag{5.4}$$

In Eq. 5.4, p is the order of convergence, or the order of accuracy, and it is related to the behavior of the solution's error. Given at least three solutions corresponding to three different mesh sizes, the value of p can be estimated through the solution of Eq. 5.5, in which r is again the ratio of discrete solution mesh sizes and ε_{ij} represents the differences in the discrete solutions, or $f_i - f_j$.

$$\frac{\varepsilon_{23}}{r_{23}^p - 1} = r_{12}^p \left(\frac{\varepsilon_{12}}{r_{12}^p - 1} \right) \tag{5.5}$$

For each of the forging, machining, and welding process simulations, discrete solutions for the the residual stresses at appropriate model locations were found for three levels of mesh refinement. Figures 5.3 and 5.4 show the mesh levels investigated, as well as the model locations probed for the residual stresses. Note that the locations at which the stresses were probed were selected as relevant to each of the processes being modeled. Specifically, the stress probe locations for the forging and machining steps provide an indication of the internal residual stress states and the location probed during the welding process corresponds to a site along the fusion interface.

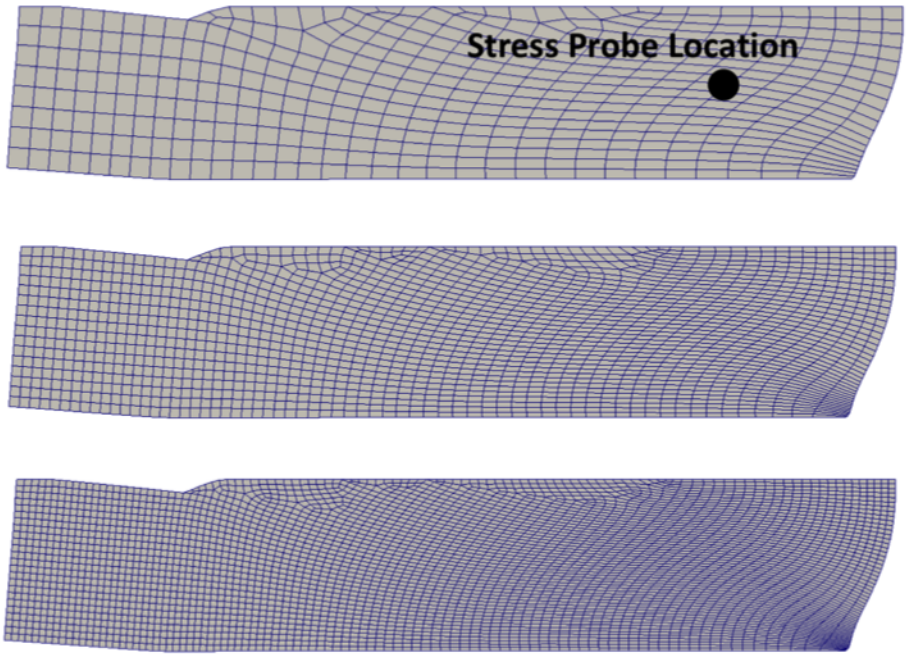

Figure 5.3. Three mesh levels investigated (forging)

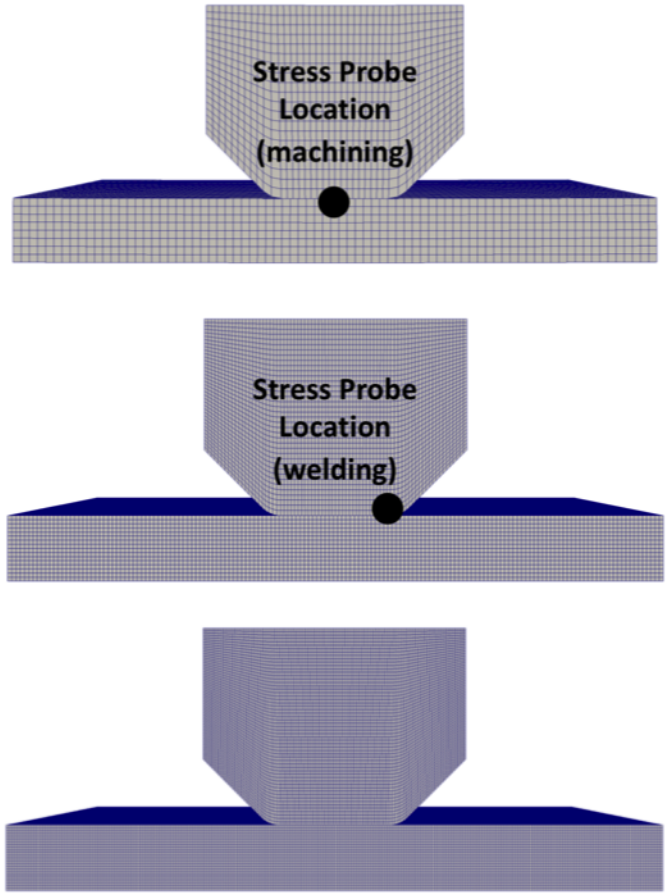

Figure 5.4. Three mesh levels investigated (machining and welding)

With the discrete solutions corresponding to the models shown in the figures above, the Richardson's extrapolated exact solutions were estimated for the residual stress levels resulting for each of the forging, machining, and welding processes with Eq. 5.4 and 5.5. Tables 5.1 through 5.3 provide a summary of the extrapolated results.

Table 5.1. Forging process Richardson's extrapolation summary

Simulation	Element Size (elements/inch)	Simulated Residual Stress (f_k)	p	Predicted Exact Solution
1	8	220.0 Msi	2.237	221.9 Msi
2	16	217.1 Msi		
3	24	199.5 Msi		

Table 5.2. Machining process Richardson's extrapolation summary

Simulation	Element Size (elements/inch)	Simulated Residual Stress (f_k)	p	Predicted Exact Solution
1	40	-66.0 Msi	3.552	-16.8 Msi
2	80	-21.0 Msi		
3	120	-17.8 Msi		

Table 5.3. Welding process Richardson's extrapolation summary

Simulation	Element Size (elements/inch)	Simulated Residual Stress (f_k)	p	Predicted Exact Solution
1	40	-118.6 Msi	2.000	-511.0 Msi
2	80	-412.6 Msi		
3	120	-467.0 Msi		

Finally, with the extrapolated continuum stress solutions shown in the tables above, the individual discretization errors associated with each of the process steps were determined with Eq. 5.6 and plotted as a function of element size. Figures 5.5, 5.6, and 5.7 show the relationship between discretization error and element size for the forging, machining, and welding processes, respectively.

$$\text{discretization error} = \frac{f_{exact} - f_k}{f_{exact}} \cdot 100 \tag{5.6}$$

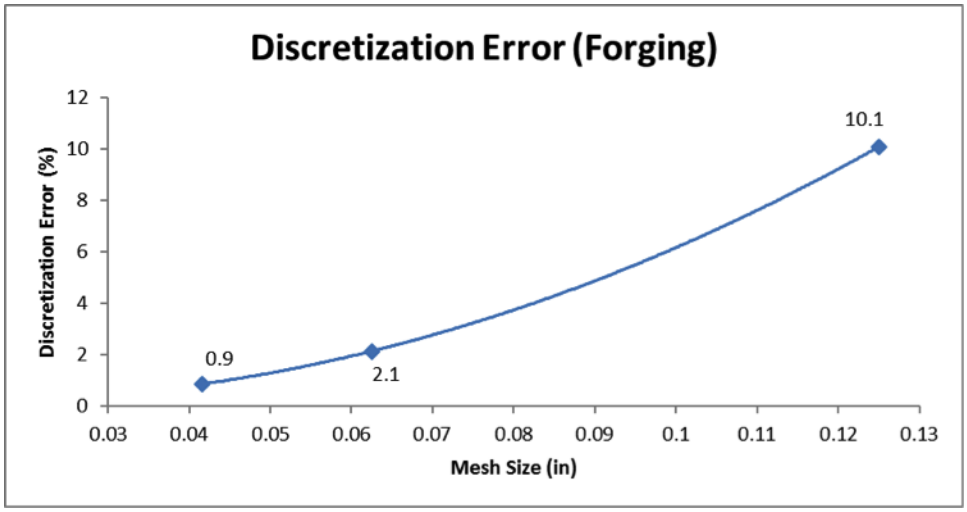

Figure 5.5. Discretization error as a function of mesh size for the forging simulation

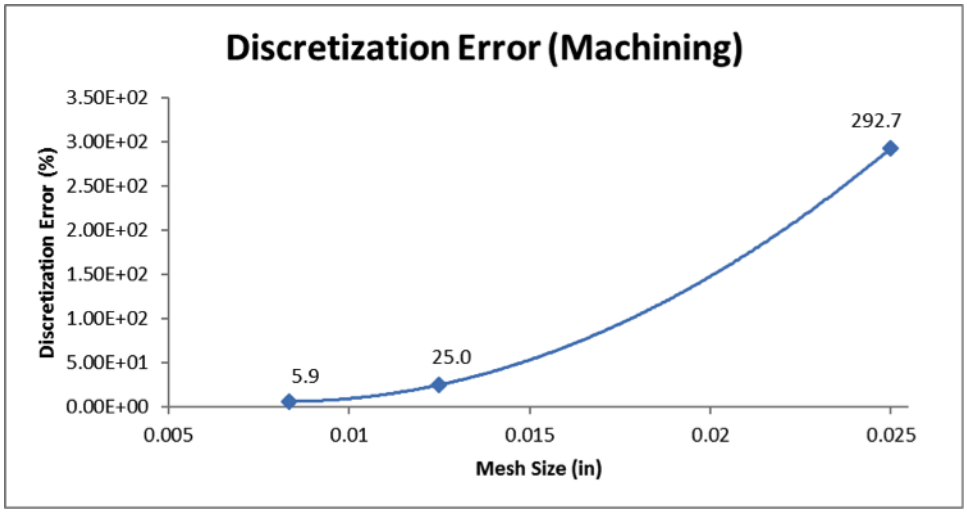

Figure 5.6. Discretization error as a function of mesh size for the machining simulation

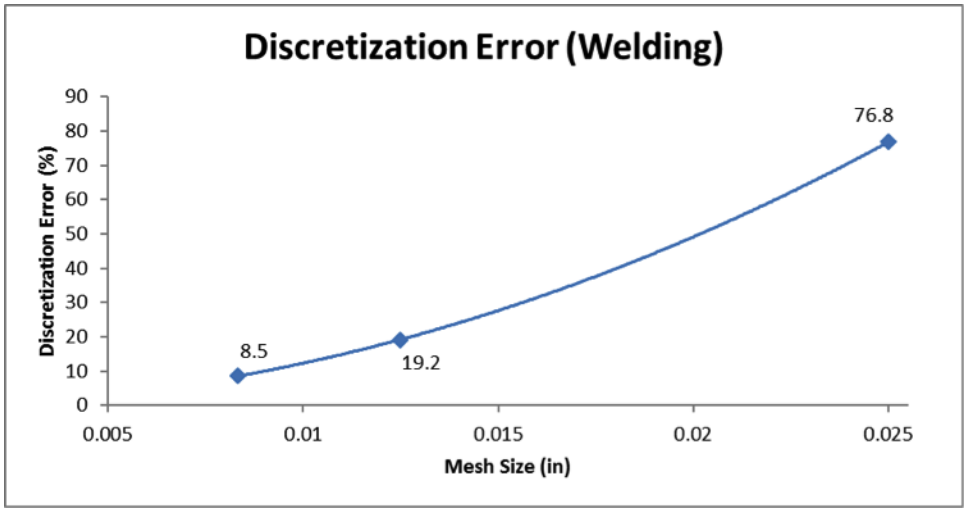

Figure 5.7. Discretization error as a function of mesh size for the welding simluation

As shown in the above tables and plots, the discretization error decreases with each level of mesh refinement, indicating that the simulations represented by the models shown in Figures 5.3 and 5.4 are converging to the extrapolated exact values and this lends confidence to the modeling procedure. Also, as shown in Figures 5.5 through 5.7, while the coarsest mesh provides an acceptably low discretization error ($< 10\%$) for the forging process, both the machining and welding simulations are verified for only the finest discretization level. Therefore, in investigations of only the forging response, the coarsest mesh can be used with confidence, while predictions of either the machining or welding behaviors must be made with the finest discretization level examined.

Chapter 6

Application Validation

The validation activities have been somewhat limited for the current manufacturing process, but the modeling capabilities provide an avenue on which future experiments can be conducted for validation. To date, the validation approach for the current work consists primarily of four activities: i.) validation and calibration of the material model, ii.) validation of the displacements for machined wedge forging, iii.) validation of the residual stress predictions and iv.) validation of the recrystallization, hardness/yield strength and thermal history for a ucup geometry that was forged, machined and then welded.

6.1 Validation of the material model

The material model utilized in the process modeling presented here accounts for rate and temperature dependence, while tracking the evolution of static and dynamic recrystallization [1]. Validation of this is documented in more detail in [3], where it demonstrated accurate predictions of the yield strength for multiple locations in different forged geometries at different temperatures. Here, the same set of parameters is used throughout the simulations.

6.2 Validation of displacements in forging and machining process

In FY13, the ability to model the machining operation of a forged weld geometry was demonstrated and validated. Computationally, after the forging is cooled to room temperature, the stress state is mapped to a mesh of the "machined" geometry. The machined part is then allowed to relax to the equilibrium state through a Sierra Presto simulation with mass damping to increase the time step. Experimentally, electrical discharge machining was used to remove tensile specimens from the forged wedge. Warpage occurred due the relaxation of the residual stresses in the wedge, creating a step in the bottom of the machined wedge. Simulation predictions of the step and of three other final dimensions agree well with the corresponding experimental measurements (see Figure 6.2).

During FY16, the aforementioned machining technique was improved by performing an L2

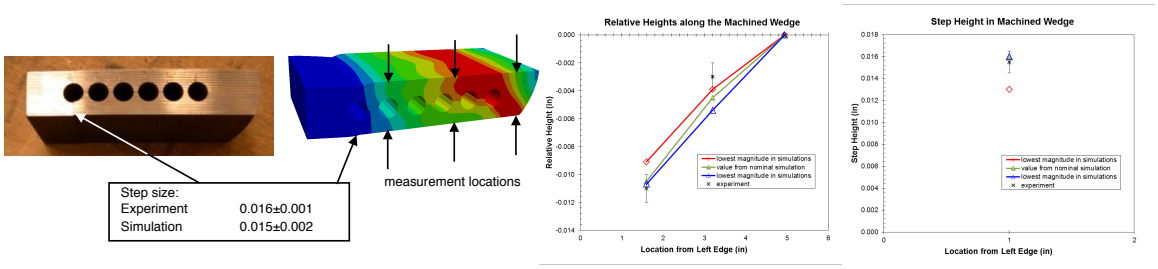

Figure 6.1. Comparison of predicted displacements with the experiment for a forged and machined wedge

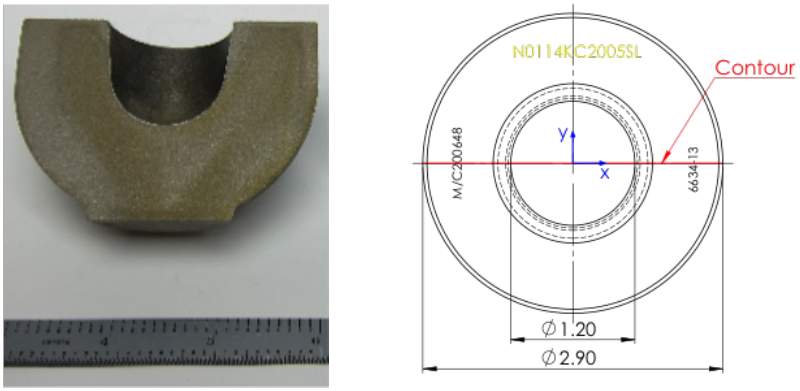

Figure 6.2. Ucup geometry for residual stress measurements

projection [8] now within the Sierra Solid Mechanics production code, rather than averaging the previous stresses on the new mesh using MAPVAR [17]. The methodology further benefited by converting the relaxation step from explicit dynamics (Presto) to implicit quasistatics (Adagio) to remove the mass scaling and damping that were previously necessary to obtain a solution. Additionally, this conversion helped improve accuracy of the solution and reduce runtime.

6.3 Validation of residual stresses in forging process

During Q2 of FY16, we demonstrated the ability to model and predict residual stress profiles for a series of ucup forgings shown in Figure 6.3 using the thermal-mechanical modeling process studied in this work. Due to some uncertainty in the time to transfer from the die to the quench bath, which has been shown to induce recrystallization in the past, a nominal case and a longer transfer time were studied. At the same time, the out-of-plane stresses were measured by Hill Engineering on this plane using the contour method by cutting the forged geometry along the centerline on the xz-plane of Figure 6.3.

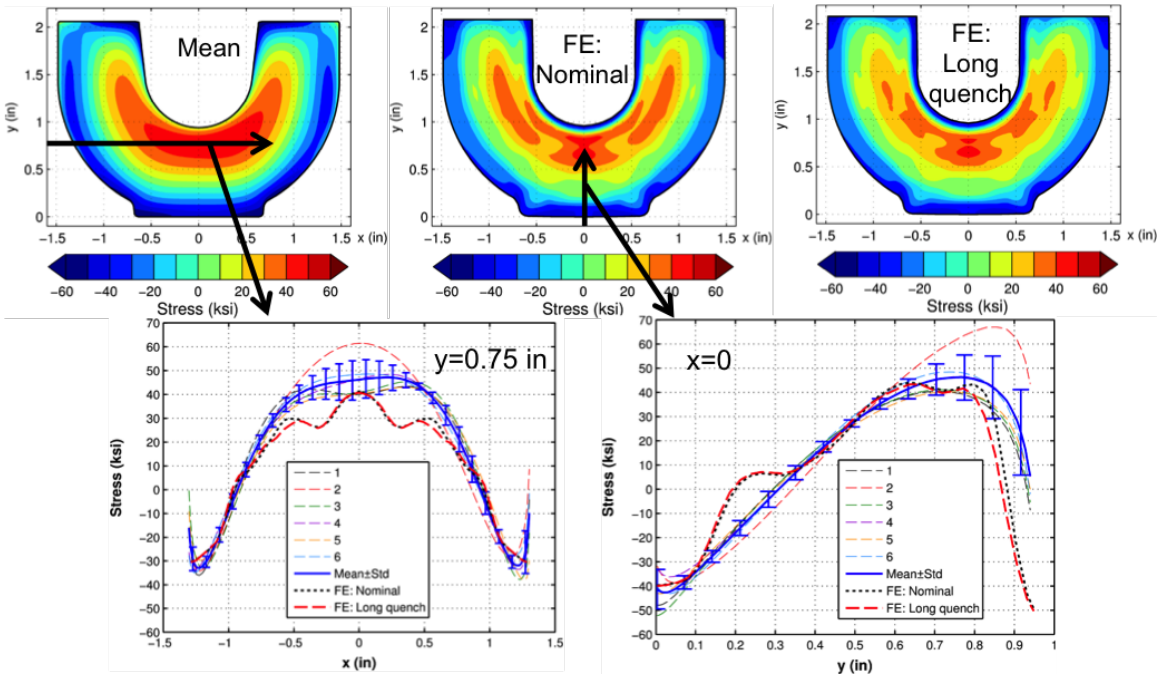

Figure 6.3. Comparison of predicted residual stress measurements for forged ucup (courtesy of Hill Engineering)

A blind comparison was made between the experiment and the modeling approach, which revealed good agreement in terms of the general trends, in addition to the magnitude and location of maximum stress (see Figure 6.3). Hole drilling measurements will be conducted next FY to better understand the discrepancies and a journal publication of the results will follow. For more details on the process and additional qualitative validation activities of the residual stress in various forgings, we refer the reader to [13].

6.4 Validation of recrystallization, yield strength and thermal history in forging, machining and welding process

In FY15, the forging, machining and welding process was studied and validated for a ucup geometry in [2] shown in Fig. 6.4. In this work, the forging process was modeled as in previous efforts, but in this case, the forging was annealed then flattened to a 2" diameter and forged at 1525F. After quenching and allowing it to come to equilibrium, a 0.25" thick slice was machined off the center of the forged ucup geometry. The slice was then placed between two platens and a GTA weld was performed at 130 A at a travel speed of 2.5 inches per second. The setup of the experiment is given in Figure 6.5. To model the process, the machining was performed using a previous mapping methodology based on the tool in [17] to transfer the state onto the new mesh. Then, for the welding, a traveling heat source was applied along the welding path.

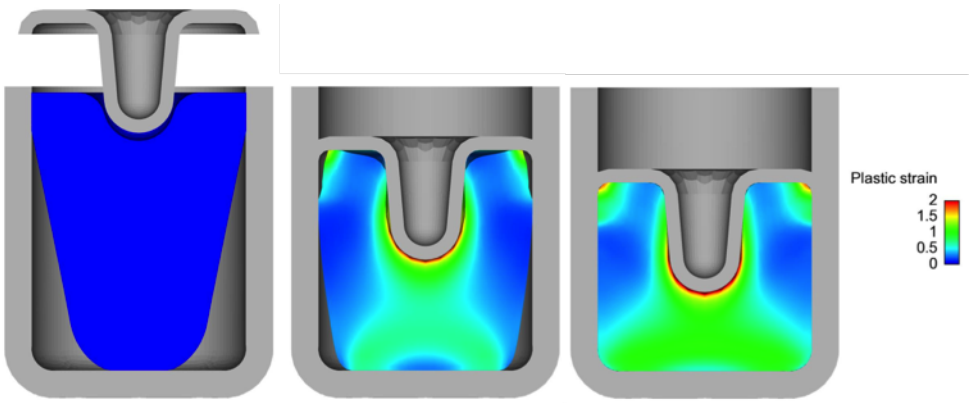

Figure 6.4. Setup of ucup forging geometry

During the experiment, five thermocouples were spot welded in the locations shown in Figure 6.5 to record the thermal history. In the modeling process, the tabs (shown above and below the slice) and clamps (not pictured) were included to allow for heat dissipation from the slice. The heat flux input was optimized in the simulation to match the thermal history at the same locations, shown in the adjacent plot.

Metallography was performed on the as-forged and welded specimens, and Vickers hardness testing was performed on polished samples. The Vickers hardness was then converted to yield strength and the results are compared in Figure 6.6 for the as-forged condition, with the markers indicating the data points. After hardness testing, the samples were then etched for microstructural imaging and the amount of recrystallization was measured by visual inspection of the grain size and shape. A comparison of the recrystallized volume fraction is shown on the right of Figure 6.6. For more detailed information on this activity, please refer to [2].

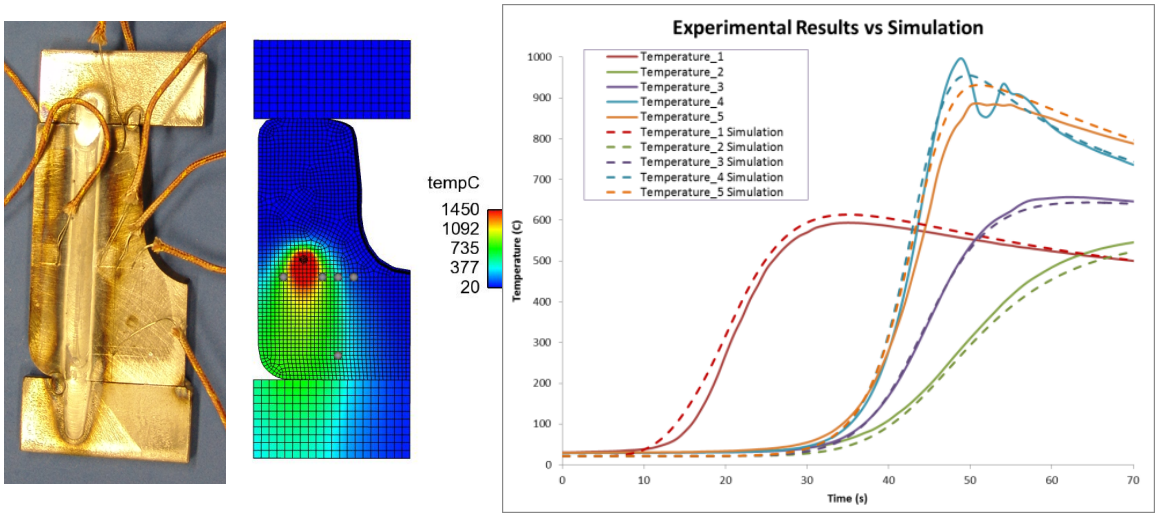

Figure 6.5. Welding setup and thermal history for forged, machined and welded ucup geometry

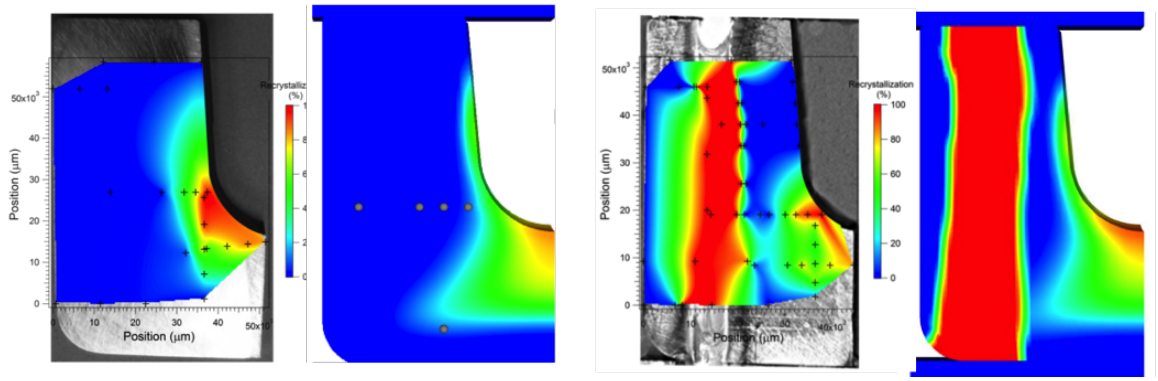

Figure 6.6. Validation of room temperature yield using hardness data as-forged (left) and recrystallization post-welding (right)

Chapter 7

Uncertainty Quantification (UQ) and Sensitivity Analysis

7.1 UQ Workflow

7.1.1 Uncertainty Quantification Approach

Due to limitation on the computation run time and resources available, the uncertainty quantification and sensitivity analysis were conducted using a Latin Hypercube Sampling (LHS) study. This allowed for maximum reuse of previous runs.

7.1.2 Sources of Uncertainties

After meeting with the customer, the key sources of uncertainty were identified as follows:

furnace temperature The temperature of the furnace in which the ingot was heated was not well controlled. Thus, a study was conducted for temperatures ranging from 1500F to 1700F, with 1600F as our nominal value.

initial platen temperature The initial platen temperature was not monitored or controlled. The range was varied from room temperature to 500F.

post forge die chill duration The time in which the hot ingot sat on the die was not controlled. A range of 1s to 30s was studied.

transfer time to quench bath The time between the end of the forging compression and the quenching was variable, and had significant effects on the recrystallization due to thermal softening (i.e. the longer the time, the more softening that would occur).

quench bath temperature The quench bath temperature was not controlled, and several forgings were quenched one after another, which could have significantly raised the temperature. Thus, we studied temperatures in the range of room temperature to 500K.

quenching convection coefficient Assumptions were made in the model on the quenching convection coefficient, as data did not exist. The range was varied between 3000 and 7000, with 5000 as the nominal value.

forging distance The distance the plates were compressed was fairly well controlled, but slightly variable. Differences in final forged heights of the wedge were observed between different lots, thus necessitating a study.

machining location The location of the machined geometry inside the original geometry was fairly well controlled, but the location could have a significant effect on the initial state of stress for subsequent process modeling steps.

welding friction coefficient With no data supplied on the frictional contact, the coefficient was varied in the simulation from 0.1 to 0.5.

displacement rate The applied displacement boundary condition for the simplified resistance weld was not based on experimental data, as it did not exist. Thus, it was varied 10% above and below the nominal value.

room temperature Assumptions were made regarding the temperature of the room in which the welding would be conducted, thus it was varied between 50F and 90F.

flux The flux boundary condition required some assumptions, as an experiment was not conducted for the welding yet at this point in time. A factor of 10% was considered.

7.1.3 Sensitivity analysis

As discussed in the preceding section, the ambiguity in several customer-defined sources must be considered during the uncertainty quantification of the forging/machining/welding process. However, given certain time and cost constraints, the complete list of parameters could not be rigorously characterized. Rather, a formal sensitivity analysis was applied to determine which of these sources of uncertainty were truly influential to the simulated residual stress response, and then only those critical parameters required thorough examination.

In initializing the sensitivity study, the twelve potential parameters described in the previous section were used to form a 12-dimensional parameter space of which the limits were defined with realistic uniform distributions for each of the provided sources of uncertainty. Table 7.1 provides these ranges, which were defined according to engineering judgment.

Table 7.1. Summary of model parameter uncertainty ranges

Model Parameter	Uniform Distribution Minimum	Uniform Distribution Maximum
Furnace Temperature	1500	1700
Initial Platen Temperature	70	500
Post Forge Die Chill Duration	1	30
Transfer Time to Quench Bath	1	30
Quench Bath Temperature	70	500
Quench Convection Coefficient	3000	4000
Forging Distance	0.95	1.05
Machining Location	-0.5	0.5
Welding Friction Coefficient	0.1	0.5
Displacement Rate	0.8	1.2
Room Temperature	283	313
Flux	0.9	1.1

After the parameter space was defined with the uncertainty ranges defined in the Table 7.1, it was sampled many times in the process of creating a set of computer experiments, or analyses, representing the simulated forging/machining/welding process models discussed in Chapter 4. Generally, the method selected to sample a parameter space must be both representative and organized to ensure that the responses corresponding to a minimum number of samples can be used to develop and recognize trends and relationships between the individual input parameters and the simulated output. Therefore, the computer experiments defined according to the described 12-dimensional parameter space were developed with a Latin Hypercube Sampling (LHS) approach. This approach was selected as, given a predefined number of sample points, the LHS method ensures that a random ensemble of sampled variables is truly representative of reality and completely covers the parameter space.

According to the mesh convergence study presented in Chapter 5, ideally, the forging, machining and welding process models corresponding to the finest mesh would be used during this sensitivity study to ensure a verified solution. However, the high computational costs associated with the most refined models was deemed prohibitive for a significant number of LHS designed simulations. Alternatively, the parameter distributions given in Table 7.1 were each sampled 40 times, creating 40 sets of sampled parameters, and these 40 parameter sets were processed through simulations of the forging/machining/welding processes using both the coarse and medium refinements discussed in Chapter 5. Upon completion of these two LHS sensitivity studies, the results corresponding to the two different meshes were assessed, as the same stress metrics upon which mesh convergence was measured (refer to section 5.2) were compared for the 40 predictions resulting from each of the coarse and medium refined models. Specifically, Figures 7.1, 7.2, and 7.3 plot the simulated stress results for the coarse mesh versus the medium mesh for the forging, machining, and welding processes, respectively.

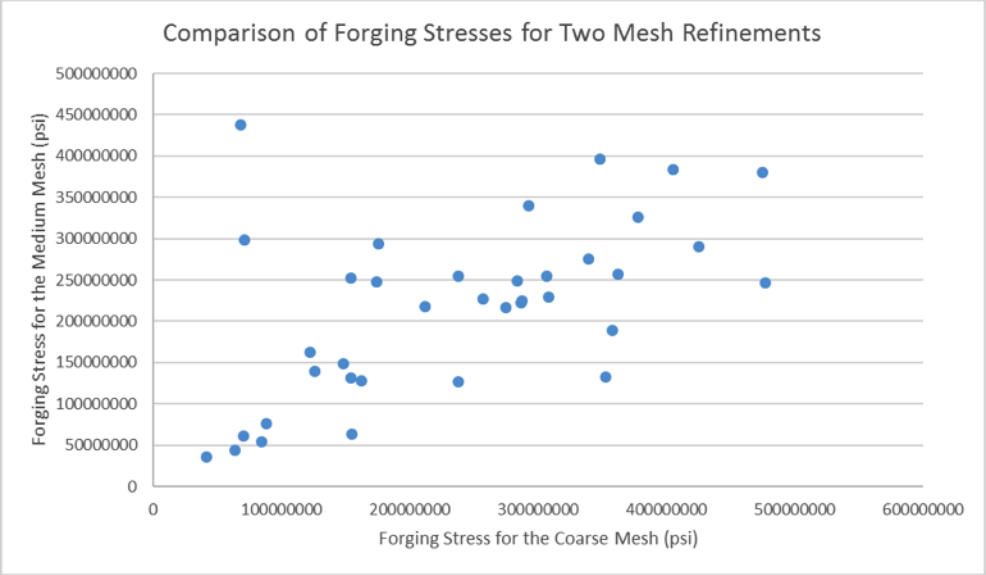

Figure 7.1. Comparison of forging residual stresses for the coarse and medium mesh refinement

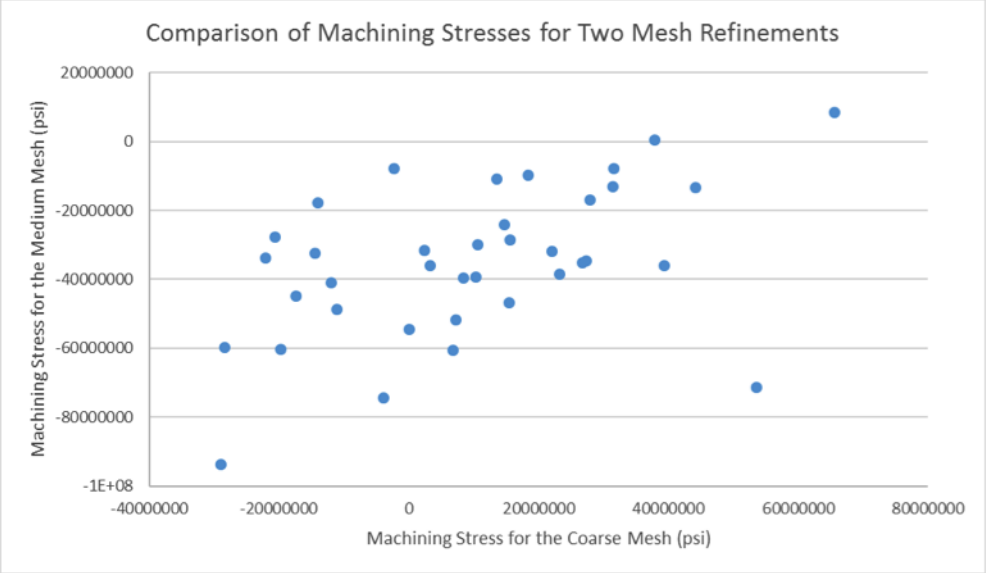

Figure 7.2. Comparison of machining residual stresses for the coarse and medium mesh refinement

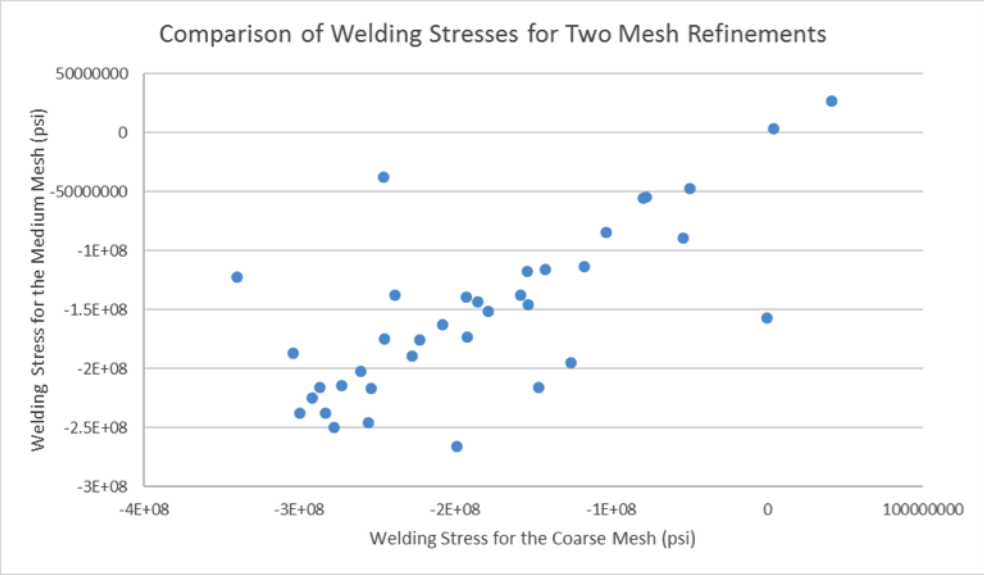

Figure 7.3. Comparison of welding residual stresses for the coarse and medium mesh refinement

As shown in the plots above, for each of the forging, machining, and welding processes, a comparison of the coarse and medium mesh refinements yields an approximately linear relationship with a heavier weight favoring neither the medium nor coarse discretizations. This indicates that trends regarding parameter sensitivity are perhaps not mesh dependent and that conclusions of which potential sources of uncertainty are most critical need not be made with the most refined mesh. Therefore, given its low computational cost, 40 additional LHS samples of the coarsely meshed forging/machining/welding model were processed, resulting in 80 total samples of the 12-dimensional parameter space. Upon completion of the 80 simulations, the individual parameter sensitivities were assessed with a multi-way analysis of variance (ANOVA), which represents a model independent, probabilistic sensitivity analysis method that can be used to determine the existence of statistical associations between an output response and one or more input parameters [9]. The completed ANOVA indicated that only 7 of the 12 potential sources of model uncertainty were critical. A summary of the ANOVA results for these 7 critical parameters is given in Table 7.2. Since the ANOVA tests the null hypothesis that the variance associated with a specific input parameter is equal to that of the overall population, low probability values, or p-values less than 0.05, indicate sufficient evidence to reject this hypothesis. Therefore, the model parameters described in Table 7.2 are demonstrably critical to the simulated response.

Table 7.2. Summary of critical model parameters

Model Parameter	ANOVA p-value
Forging Distance	0.049
Furnace Temperature	0.000
Quench Convection Coefficient	0.003
Post Forge Die Chill Duration	0.000
Initial Platen Temperature	0.011
Machining Location	0.002
Displacement Rate	0.000

The sensitive parameters summarized in Table 7.2 can intuitively be justified as critical to the formation of residual stresses throughout the forging/machining/welding process with engineering judgment. First, regarding the forging distance, this parameter outlines the extent to which the metal ingot is compressed. Instinctively, it is understood that greater amounts of compression will result in the formation larger residual stresses upon conclusion of the forging process. Next, with respect to both the furnace and initial platen temperatures, it is expected that greater temperature differentials between the ingots pre- and post- quench conditions could affect the quantity of the developed stresses. Specifically, it is possible that, with large thermal excursions, the ingot dissipates less heat away and a greater residual stress state forms as a consequence. Next, the quenching convection coefficient governs how quickly heat if transferred from the ingot during the quenching process. Therefore, it is expected that as this coefficient increases, the rate at which heat is dissipated from the ingot changes and the magnitude of the residual stresses formed through the process is reasonably affected. Next, regarding the post forge die chill duration, this parameter defines the duration of time over which the ingot remains in contact with the die prior to introduction into the quench bath. Typically, it is understood that longer pre-quench time durations promote increased recrystallization and softening within the ingot that effectively reduce the existing residual stresses. Next, the machining location represents the site from which the subset mesh is taken from the original forging geometry. Since the post-forging residual stresses are not constant over the ingots volume, it is intuitively understood that the subset mesh will exhibit higher or lower residual stresses according to the location from which they are mapped from the original ingot. Lastly, with regards to the displacement rate, this parameter defines how quickly the welding boundary conditions are applied. While the criticality of this parameter could perhaps be solver dependent, the metallic material being modeled is rate dependent. Therefore, it is possible that increasing the displacement rate will cause the material to demonstrate rate dependent behaviors with a resulting net increase in the residual stresses formed during the welding process.

7.2 Preliminary Uncertainty Quantification (UQ)

According to the sensitivity analysis described in the preceding section, seven of the original twelve potential sources of uncertainty were specified as influential to the simulated residual stress re-

sponse. Therefore, in a preliminary quantification of the uncertainties associated with just the forging process, a new parameter space was developed with the uncertainty sources related to the forging process alone. Specifically, of the critical parameters listed in Table 7.2, only the forging distance, furnace temperature, quenching convection coefficient, post forge die chill duration, and initial platen temperature were influential to predictions of the forging response. Consequently, with the same parameter ranges given in Table 7.1, a new 5-dimensional parameter space was developed and subjected to 100 new LHS samples. These 100 samples resulted in 100 parameter sets that were processed through 100 new forging process simulations in order to propagate the input parameters uncertainties through to the predicted response and fully understand what effect these five critical parameters have on the estimated residual stresses. Note that these new 100 forging process simulations were completed with the coarsest mesh shown in figure 5.1, as acceptable discretization errors were observed for all levels of mesh refinement examined during the mesh convergence study of the forging process (refer to Figure 5.3).

Upon completion of the 100 forging process simulations, the results were examined statistically in order to characterize the resulting distribution of 100 residual stress predictions. The distribution created by the 100 simulated responses was tested for normality with the adjusted Anderson-Darling statistic, which presents a method to determine how well a data set follows a particular distribution, such as a normal distribution [4]. Specifically, the Anderson Darling statistic can be calculated with Eq. 7.1 shown below:

$$AD = -N - S \tag{7.1}$$

Where, N is the number of samples and S is given by Eq. 7.2:

$$S = \sum_{i=1}^{N} \frac{(2i-1)}{N} \left[ln\left(F(Y_i)\right) + ln\left(1 - F(Y_{N+1-i})\right) \right] \tag{7.2}$$

In the equation shown above, F represents the cumulative distribution function for the specific distribution of interest, which in this case was a normal distribution. Then, the Anderson Darling statistic can be adjusted for sample size with Eq. 7.3:

$$AD^* = AD\left(1 + \frac{0.75}{N} + \frac{2.25}{N^2}\right) \tag{7.3}$$

Where, N is again the number of samples. Then, the adjusted Anderson Darling statistic can be compared to a critical value. Particularly, if AD^* is less than 0.752, the 5% hypothesis for normality is satisfied and the data set can be assumed as normal.

The above three equations were applied to the 100 forging residual stress predictions and the resulting adjusted Anderson Darling statistic was determined to be 0.520. Since this AD^* value is less than the critical value of 0.752, the predicted residual stress response distribution can be taken as normal. Therefore, a histogram and normal distribution were fit to the data set and the

mean value and standard deviation were determined. Figure 7.4 shows this histogram along with the normal distribution probability density function.

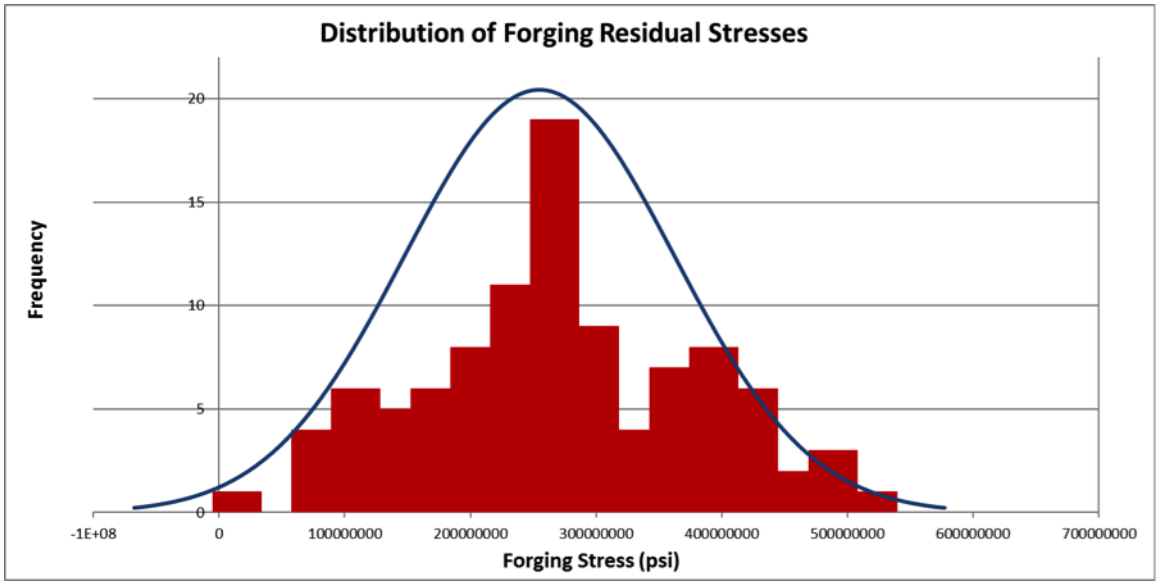

Figure 7.4. Normal distribution of the uncertainty analysis simulation output

As evident by the normal distribution shown in the plot above, the mean value was determined to be 37.0 ksi with a standard deviation of 15.6 ksi. Therefore, with the inclusion of the input parameter uncertainties discussed in Section 7.1.2, the post-forging residual stress prediction can be reported as 37.0 ksi $\pm$ 42%.

Chapter 8

Summary and Conclusions

In this work, verification and validation was performed to assess the capability to model a series of manufacturing processes while tracking the evolution of the material state and residual stresses for a forging, machining and welding process. The following conclusions can be drawn:

- Though validation activities were somewhat limited, trends were captured between the simulation results and experimental measurements. The capability presented here would benefit from more focused validation efforts, including:
  - Pointed experiments for each manufacturing step (e.g. resistance welding and machining)
  - An experiment including the entire series of steps, specifically incorporated forging, machining, heat treating and subsequent resistance welding
- Remeshing and mapping capabilities demonstrated here have significantly improved, but more V&V work is needed to understand the propagation of error resulting from mappings. The error in mesh convergence was higher for the machining and welding steps, after the mapping was performed, which requires more directed activities to explain the cause.
- Support for implicit contact through bug fixes and algorithm improvements is necessary to obtain the robustness needed to solve problems for V&V application and solution exploration purposes. For more information, please refer to [7].
- Axisymmetric elements or periodic boundary conditions could improve V&V robustness and provide huge performance gains.
- Process modeling tools enable integration with subsequent aging process
  - Future work will include linkage with tritium/helium diffusion and hydrogen embrittlement process to understand propagation of uncertainties on residual stress (see Figure 1.1) in FY17 to support the cradle-to-grave Pegpost effort.

References

[1] A.A. Brown and D.J. Bammann. Validation of a model for static and dynamic recrystallization in metals. *International Journal of Plasticity*, 32-33:17–35, 2012.

[2] A.A. Brown, L.A. Deibler, L.L. Beghini, T.D. Kostka, and B.R. Antoun. Process modeling and experiments for forging and welding. In *SEM*, 2015.

[3] A.A. Brown, T.D. Kostka, B.R. Antoun, M.L. Chiesa, D.J. Bammann, S.A. Pitts, S.B. Margolis, D. O'Connor, and N.Y.C. Yang. Validation of thermal-mechanical modeling of stainless steel forgings. In *Proc. XI International Conference on Computational Plasticity Fundamentals and Applications*, 2011.

[4] R DAugostino and M Stephen. *Goodness-of-fit Techniques*. Marcel Dekker, 1986.

[5] K Karlson and AA Brown. Computational Tools to Predict Residual Stresses in Resistance Welded Components, 2013.

[6] T. D. Kostka. Exomerge user's manual: A lightweight Python interface for manipulating exodus files. Technical report SAND2013-0725, Sandia National Laboratories, Albuquerque, New Mexico 87185 and Livermore, California 94550, january 2013.

[7] K.L. Manktelow and L.L. Beghini. Development of a Multi-physics Capability for Predicting Residual Stress in a GTS Reservoir. Technical report SAND2016-9071, Sandia National Laboratories, Albuquerque, NM and Livermore, CA, 2016.

[8] A. Mota, W. Sun, J.T. Ostien, J.W. Foulk, and K.N. Long. Lie-group interpolation and variational recovery for internal variables. *Computational Mechanics*, 52(6):1281–1299, 2013.

[9] NIST/SEMATECH. Engineering Statistics Handbook [Online], 2013.

[10] W.L. Oberkampf, M. Pilch, and T.G. Trucano. Predictive capability maturity model for computational modeling and simulation. Technical report SAND2007-5948, Sandia National Laboratories, Albuquerque, New Mexico 87185 and Livermore, California 94550, 2007.

[11] W.L. Oberkampf and C.J. Roy. *Verification and Validation in Scientific Computing*. Cambridge University Press, New York, 2010.

[12] Sierra Product Owners. Sierra Support for PCMM. Technical report, Sandia National Laboratories, Albuquerque, NM, 2013.

[13] T.B. Reynolds, A.A. Brown, L.L. Beghini, T.D. Kostka, and C.W. San Marchi. Development of Residual Stress Simulation and Experimental Measurement Tools for Use in Lifetime Assessment of Stainless Steel Pressures Vessels. In *Proceedings of the 14th International Conference on Nuclear Engineering*, 2015.

[14] P Roache. A Method for Uniform Reporting of Grid Refinement Studies. *J Fluids Eng*, 116:405–413, 1994.

[15] P Roache. Verification of Codes and Calculations. *AIAA J*, 36:696–702, 1998.

[16] V&V/UQ Team. How to PIRT. Technical report SAND2013-6285P, Sandia National Laboratories, Albuquerque, New Mexico 87185 and Livermore, California 94550, 2013.

[17] G.W. Wellman. MAPVAR - A Computer Program to Transfer Solution Data Between Finite Element Meshes. Technical Report SAND99-0466, Sandia National Laboratories, Albuquerque, New Mexico 87185 and Livermore, California 94550, 1999.

DISTRIBUTION:

1	MS	9042	Beghini, Lauren, 08259
1	MS	9042	Brown, Arthur, 08259
1	MS	9159	Hough, Patricia, 08954
1	MS	9152	Lefantzi, Sophia, 08954
1	MS	9042	Manktelow, Kevin, 08259
1	MS	9042	Nelson, Stacy, 08259
1	MS	9042	Nilsen, Curt, 08250
1	MS	0825	Payne, Jeffrey, 01513
1	MS	9042	Peterson, Scott, 08343
1	MS	0845	Pierson, Kendall, 01542
1	MS	0840	Scherzinger, William, 01554
1	MS	0899	Technical Library, 8944 (electronic copy)


Sandia National Laboratories